Resolution of Multiphasic Reactions by the Combination of Fluorescence Total-Intensity and Anisotropy Stopped-Flow Kinetic Experiments

Michael R. Otto, M. Pilar Lillo, and Joseph M. Beechem
Department of Molecular Physiology and Biophysics, Vanderbilt University, Nashville, Tennessee 37232 USA

ABSTRACT Multiphasic kinetics are often observed in stopped-flow investigations. To characterize further these kinetic phases, we have developed a methodology whereby fluorescence total intensity and anisotropy stopped-flow data can be combined in a single analysis. Fluorescence total intensity and anisotropy are highly interrelated and contain two very complementary forms of information. Total-intensity changes are useful in determining changes in populations with differing quantum yields, whereas anisotropy changes contain additional contributions caused by the rotational dynamics of the species. For cases in which the fluorescence quantum yield increases, the observed rate of anisotropy change will be more rapid than the total-intensity change, whereas in cases in which the total intensity decreases, the observed change in anisotropy will lag behind. In all cases, with quantum yield changes the stopped-flow anisotropy signals cannot be fit with models consisting of exponentials. Case studies examining these effects are described for the protein folding/refolding transitions of *Staphylococcal* nuclease and phosphoglycerate kinase. A multiphasic DNA exonuclease reaction using bacteriophage T4 DNA polymerase is also examined. In all of these cases, combined analysis of both data types revealed insights into reaction mechanism, which could not be obtained by either data type in isolation. Quantum yields and steady-state anisotropies associated with transiently populated intermediate species can be resolved. The data analysis methodologies described allow characterization of multiphasic reactions in terms of internally consistent kinetic rates, quantum yields, and steady-state anisotropies.

INTRODUCTION

Fluorescence spectroscopy is often utilized as a method to follow stopped-flow reactions because of its inherent sensitivity and timing resolution. The two basic types of fluorescence data that are usually examined are total-intensity and steady-state anisotropy (SSA). Both types of data contain information concerning changes in the relative populations of species during a reaction. However, steady-state anisotropy data contain additional information describing the average molecular motion that occurs during the lifetime of the excited-state. For protein folding reactions, this additional information provides a manner in which the average hydrodynamic properties of folding intermediates can be obtained. Although the rigorous combination of both total-intensity and anisotropy stopped-flow data to help understand complex reaction mechanisms would appear beneficial, no studies of this type have been reported to date.

Total-intensity and SSA data have been used in conjunction in the past to obtain more information about ligand-receptor interactions than was present in the two types of data alone (Levison, 1975; Dandliker et al., 1978; Dandliker et al., 1981). In these studies, the combined anisotropy and intensity information was used to determine the reaction order and association/dissociation rate constants. These methods utilized analytical forms for the stopped-flow anisotropy function that were only appropriate for the initial time-points of the reaction. Our study extends these works in a manner that allows simultaneous analysis of total-intensity and anisotropy stopped- flow data over complete time-courses and any concentration range. From this analysis, additional information concerning the total number and physical properties of intermediate states are obtained. Protein unfolding and refolding reactions are examined as test cases, as well as a DNA polymerase reaction.

MATERIALS AND METHODS

Materials

Staphylococcal nuclease Δ114–119 mutant was a gift from Dr. David Shortle (The Johns Hopkins University, Baltimore, MD). Yeast (*S. cervesiae*) phosphoglycerate kinase wt and single tryptophan mutant, W48, were gifts from Dr. Maria Mas (Beckman Research Institute of the City of Hope, Duarte, CA). Bacteriophage T4 DNA polymerase was a gift from Dr. Linda Reha-Krantz (University of Alberta, Edmonton, Alberta, Canada). The pAP/tTT primer/template DNA used for T4 excision experiments was prepared as in Bloom et al. (1994).

Methods

Stopped flow fluorescence detection

Reactions were performed with an SFM-3 stopped flow unit (Molecular Kinetics, Pullman, WA) with a 50 μl FC.15 fluorescence cuvette and hard-stop shutter. Reaction flow rates varied from 2 to 8 ml/s. Reaction time bases depended upon the experiment. Stock solutions of enzyme, dilution buffer, and reaction buffer were loaded into separate syringes. For all experiments, solutions were extensively degassed. All experiments were collected with a fraction of the data channels devoted to internal controls. For folding and unfolding reactions, the internal controls were simply unfolded or folded protein, respectively. The internal control for DNA polymerase reactions

Received for publication 28 June 1994 and in final form 3 October 1994.

Address reprint requests to Dr. Joseph M. Beechem, Department of Molecular Physiology /Biophysics, Vanderbilt University, 702 Light Hall, Nashville, TN 37232. Tel.: 615-343-7687; Fax: 615-322-72-36; E-mail: beechem@vulhmrba

Dr. Lillo's current address: Instituto de Quimica Fisica, CSIC, Serrano 119, E-28006 Madrid, Spain.

0006-3495/94/12/2511/11 $2.00

utilized pre-bound T4/DNA complex in the absence of Mg^{2+}. These control reactions had absolutely flat anisotropy and total- intensity signals. This control region of total-intensity data was utilized to normalize the observed total-intensity change of the reaction (see term C in Eqs. 6 and 8 below).

A T-format steady state anisotropy fluorimeter was assembled using the following components. The excitation beam was provided by a 450 W Xenon Arc lamp with a 0.22m SPEX monochromator (Edison, NJ) whose output was focused onto a fused-silica fiber optic (10 × 100 μm fiber bundle) and directed into the 50 μl stopped-flow observation cuvette after passing through a vertically oriented Oriel film uv linear dichroic polarizer (Stratford CT, model 27340). On each side of the SFM-3 cuvette head, a homemade emission channel was mounted, consisting of a collimating lens, Glan-Thompson polarizer and filter holder. The filters utilized were either 340 or 360 nm cut on type (L34 or L36, Hoya optics, Fremont, CA). On the end of each emission channel, a R928 photomultiplier tube (PMT) (Hamamatsu Corp.) operating in single-photon counting mode was mounted. Signal from each PMT (measuring light polarized either parallel or perpendicular to the excitation beam) was amplified through an SR455 DC-300 amplifier (Stanford Research, Sunnyvale, CA) and discriminated with an SR400 (Stanford Research) two channel counter. The parallel and perpendicular intensities were simultaneously detected by two MCS-II multichannel scalar cards (Tennelec Nucleus, Oak Ridge, TN) and two 486DX computers. The MCS-II cards were synchronized with the SFM-3 stopped-flow unit through the external sync output from the SFM-3. The excitation polarizer in this stopped-flow instrument is "sandwiched" between the front surface of the observation cuvette and the excitation fiber optic and cannot be easily rotated for horizontal excitation to determine the polarization bias ("*G*-factor") of the instrument (Eqs. 1 and 2 below). Therefore, the *G*- factor is obtained by measuring a sample with a known steady- state anisotropy (e.g., dAPMP in solution has a steady-state anisotropy of essentially 0.0) and solving for *G*. A 30 μM solution of free tryptophan was utilized for folding reactions, and 1 μM 2-aminopurine monophosphate was used for exonuclease reactions. All reactions were performed at 20 ± 2°C. Multiple kinetic runs were summed (10–15) to obtain adequate signal-to-noise ratios. Anisotropy and total intensity data were obtained from the parallel and perpendicular channel data using Eqs. 1 and 2 (see below).

Excitation source for T4-DNA Mg^{2+} initiated kinetics

For the anisotropy experiments in this study, the excitation light source was a 306 nm beam supplied by the frequency doubled output from a Coherent 702 dye laser being pumped by a 532 nm beam from a Coherent Antares Nd:YAG laser (Coherent, Inc, Palo Alto, CA). This 306 nm excitation beam was used to excite 2AP within DNA, and the emission was collected using a 360 nm cut on filter.

Determination of the refolding rate of Staphylococcal *nuclease deletion mutant*

Rate of folding was determined from increase in tryptophan fluorescence (W140, λ_{ex} = 295 nm), and the emission was collected using a 340 nm cut on filter. Time base for the reaction was 125 ms/channel. Reactions were performed by mixing 100 μl of nuclease mutant stock (pH = 3.2) with 400 μl of reaction buffer with the final pH being 7.0. Reaction buffer was 0.1 M sodium phosphate, pH 8.2. All reactions contained 0.16 mg/ml Δ114–119 nuclease mutant, 85 mM sodium phosphate, and 8 mM sodium-citrate, pH 7.0.

Determination of the unfolding rate of Staphylococcal *nuclease deletion mutant*

Rate of unfolding was determined from decrease in tryptophan fluorescence using conditions as described above in refolding experiments. Time base for the experiment was 35 ms/channel. Reactions were performed by mixing 100 μl of nuclease stock in 0.1 M sodium phosphate (pH = 7.0) with 400 μl reaction buffer. Reaction buffer was 25 mM sodium phosphate/38 mM sodium citrate, pH 3.0. All reactions contained 0.16 mg/ml nuclease mutant, 30 mM citrate, and 40 mM sodium phosphate, pH 3.6.

Determination of the unfolding rate of wt yeast phosphoglycerate (PGK) kinase

Rate of unfolding was determined from increase in tryptophan fluorescence as described in the nuclease experiments above. Wild-type PGK has two tryptophan residues at positions 308 and 333. Time base of detection was 25 ms/channel. Reactions were performed by mixing 100 μl PGK stock with 225 μl 2.0 M GuHCl. All reactions contained 50 mM MOPS, 100 mM NaCl, 0.062 mg/ml phosphoglycerate kinase, 1.4 M GuHCl.

Determination of the pre-unfolding rate of W48 single tryptophan PGK mutant

As above in the wild-type PGK study, the rates of reaction were determined from increase in tryptophan fluorescence from a single tryptophan at position 48. The W48 mutant is actually a triple mutant with phenylalanines replacing the tryptophan residues at positions 308 and 333. Time base of detection was 50 ms/channel. Reactions were performed by mixing 100 μl PGK stock with 100 μl 1.0 M GuHCl. All reactions contained 50 mM MOPS, 100 mM NaCl, 0.1 mg/ml W48 mutant, 0.5 M GuHCl.

Determination of the reaction rates for the excision of DNA by T4 exonuclease: Mg^{2+}-initiated reactions

This particular experiment was performed utilizing the DNA polymerase from the T4 bacteriophage and a synthetic primer/template (P/T) (17/30mer, pAP/tTT) with the fluorescent nucleotide 2-aminopurine monophosphate (dAPMP λ_{ex} = 304 nm) at the 3′ end of the primer. The T4 polymerase has 3′-5′ exonuclease activity and upon excision from the primer (single product turnover being visualized) the 2-aminopurine base (2AP) undergoes an enormous change (25–125-fold) (Bloom et al., 1994) in relative quantum yield. Time bases for the reaction were 0.25 ms/channel for anisotropy experiments and 1 ms/channel for intensity experiments. Reactions were performed by mixing 100 μl of $MgCl_2$ with 100 μl T4 polymerase : DNA complex stock at 8 ml/s with a measured dead time value of 7.4 ± 1.0 ms. The dead time was measured as in Bloom et al. (1994). To increase signal-to-noise in the intensity analysis, separate intensity and anisotropy data sets were collected, and the measured light intensity was corrected to the actual total intensity using the known change in steady-state anisotropy and Eq. 11 in the Appendix. Combined intensity and anisotropy analysis was then performed. Reactions were initiated by mixing 400 nM T4 polymerase-DNA complex (in 0.5 mM EDTA to inhibit exonuclease activity) with 16 mM $MgCl_2$. All reactions contained 8 mM $MgCl_2$, 25 mM HEPES, pH 7.5, 50 mM NaCl, 0.25 mM EDTA, 200 nM DNA, and 680 nM T4 polymerase.

Determination of kinetic rates

Empirical exponential fits to single exponentials or sums of exponentials were performed using Sigmaplot 4.1 (Jandel Scientific, San Rafael, CA). Combined global analyses were performed using the Globals Unlimited software package (Urbana, IL; modified to include the theory/methods developed in this work), which is based upon the Marquardt-Levenberg nonlinear least-squares algorithm and compartmental eigenvector/eigenvalue problem solver. Some of the three state models utilized in this paper are shown in Chart I. The fitting parameters for each reaction scheme consist of reaction rates, quantum yields, and steady-state anisotropy values associated with each particular chemical species. Full details concerning the data analysis are provided below.

THEORY

The steady-state fluorescence total intensity and anisotropy functions when exciting sample with vertically polarized

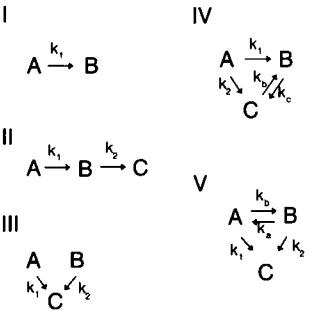

CHART I. Unimolecular kinetic reaction schemes. Population of each species were obtained from solution of the compartmental eigenvector/eigenvalue problem. For scheme III, an analysis term describing the initial populations of A and B was also utilized.

light are given in Eqs. 1 and 2, respectively:

$$S = GI_{\parallel} + 2I_{\perp} \quad (1)$$

$$r = (GI_{\parallel} - I_{\perp}) / (GI_{\parallel} + 2I_{\perp}), \quad (2)$$

where $I_{\parallel}$ and $I_{\perp}$ are the intensities of fluorescence emitted parallel and perpendicular to the exciting light. G (G-factor) is a term accounting for the bias of the detection system for vertical versus horizontally polarized light.

In kinetic experiments the fluorescence total intensity is described by

$$S(t) = \Sigma x_i(t)\epsilon_i(\lambda_{ex})f_i(\lambda_{em})\, q_i = \Sigma x_i(t)q_i^{eff}, \quad (3)$$

where x_i, ϵ_i, f_i, and q_i are the fraction of total observed species in state i at time t, the molar extinction coefficient (ϵ_i) at the excitation wavelength, fluorescence spectral contour (f_i) at the emission wavelength(s) collected, and the quantum yield of state i, respectively. For stopped-flow experiments performed at a single excitation/emission bandpass, the three terms $\epsilon_i(\lambda_{ex})f_i(\lambda_{em})$ and q_i, can be collapsed into a single effective term q_i^{eff}. The advantage of performing the data analysis in terms of effective quantum yields is that the initial data analysis is greatly simplified without sacrificing any loss of information.

The observed anisotropy will be described as

$$r(t) = \Sigma x_i(t)q_i^{eff}r_i / \Sigma x_i(t)q_i^{eff}, \quad (4)$$

where x_i and q_i^{eff} are as in Eq. 3 and r_i represents the steady-state anisotropy values of species i. It should be emphasized that $S(t)$ will follow exponential (or multi- exponential) behavior, whereas $r(t)$ is strictly nonexponential (i.e., is not correctly described using exponentials), except in the case where the quantum yields of all states are equal. Equation 4 is formally equivalent to the time- resolved fluorescence anisotropy equation for the strictly "associative" case (Ludescher et al., 1987), which has been shown to have no exact general analytical solution (Brand et al., 1985).

Equation 4 shows that the SSA can be heavily influenced by differences in the effective quantum yields (q^{eff}) of the various species present during a reaction. In this situation, the change in SSA will not accurately represent the change in populations over time (Eftink, 1994). In reactions where both a change in SSA and total intensity occurs, the SSA time course and rate must differ from those observed for the total intensity. This will be demonstrated in the Discussion. It must be noted that the observed intensity is also subject to the value of the steady-state anisotropy and if natural (without polarizers) emitted light is observed one must be careful to correct for polarization bias effects. This is discussed in the Appendix.

Because the time course of a stopped-flow anisotropy experiment cannot be represented analytically, numerical methods are required. Fortunately, for many stopped-flow experiments, the actual populations ($x_i(t)$) are exponential and can be solved for using either analytical solutions or through general-purpose eigenvector/eigenvalue solving routines. We have found it very convenient to utilize the EISPACK set of eigenvector/eigenvalue routines within a general purpose compartmental analysis framework (Beechem et al., 1991). Combined stopped-flow fluorescence total-intensity and anisotropy analysis is performed in the following manner (see Chart II).

1) Boundary conditions and initial parameter values are entered for the rate constants linking the various chemical

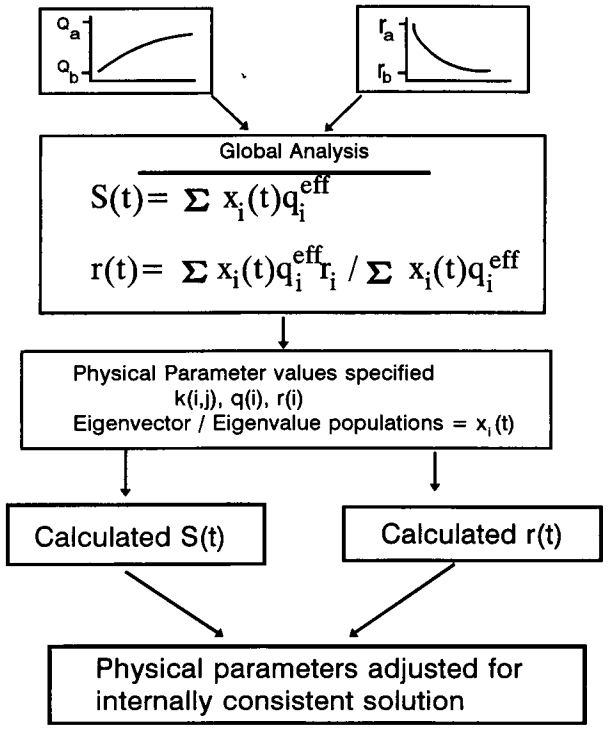

CHART II. Flow chart for combined fluorescence intensity and anisotropy analysis. The total intensity ($S(t)$) and anisotropy ($r(t)$) data are imported into the analysis routine. Initial parameter values (x_i, q_i, r_i) and boundary conditions are entered. An eigenvalue/eigenvector problem solver is used to generate populations of the species as a function of time. Both the population terms ($x_i(t)$) and quantum yield terms are common to both data types and are constrained to be internally consistent during data analysis. Calculated observables are then obtained from initial parameter values and the generated populations. These calculated observables are then compared with the imported data, and if a χ^2 minimum is not obtained the parameters are altered and another iteration is initiated. For a full description see Theory section

species. Initial guesses for the quantum yields and SSA values associated with each state are entered.

2) Given the kinetic rate constants and boundary conditions, an eigenvalue/eigenvector solver is used to construct the populations $x_i(t)$.
3) Using these calculated populations and the initial guesses for the intensity (q_i^{eff}) and anisotropy observables (r_i), Eqs. 3 and 4 are utilized to generate the total-intensity and anisotropy observables.
4) These calculated observables are then compared with the experimental data to obtain a χ^2 value (Eq. 5).
5) Fitting parameters are then adjusted to minimize the χ^2 value.

The important point to note in this fitting procedure is that the actual population terms ($x_i(t)$) and quantum yield terms (q_i^{eff}) are linked between the two data sets. The properly weighted global χ^2 that is minimized in these experiments is

$$\chi^2 = \sum_{j=1}^{nexp} \sum_{i=1}^{n(j)} \frac{(d_{ji} - f_{ji})^2/\sigma_{ji}^2}{(N - M - 1)}, \quad (5)$$

where d_{ji} and f_{ji} are the observed data and fit for the ith point of the jth experiment, N = total number of data points (sum of both total- intensity and anisotropy traces), σ_{ji} = SD of the data, M = total number of fitting parameters, $n$exp = the total number of experiments being analyzed. Utilization of the correct weighting terms (see below) yields χ^2 values at optimal fitting that will approach 1.0.

The measured quantities in these experiments are $I_\parallel$ and $I_\perp$, and the noise on these observables is simply $(d_{ji})^{1/2}$. Data analysis, however, is being performed in terms of the $S(t)$ and $R(t)$ functions defined above. When combining the experimental total-intensity and anisotropy decay functions, one must properly "weight" each data set. Fortunately, the SD weights for fluorescence total-intensity and anisotropy can be calculated exactly as per Bevington and Robinson (1992), and first performed by Wahl (1979) for nanosecond time-resolved fluorescence data. The functional form for the stopped-flow total-intensity (σ_s^2) and anisotropy functions (σ_r^2) are identical to the time-resolved fluorescence cases:

$$\sigma_s^2 = \frac{G^2(I_\parallel + B_\parallel) + 4(I_\perp + B_\perp)}{C^2} \quad (6)$$

$$\sigma_r^2 = \frac{[G(I_\parallel - B_\parallel) - (I_\perp - B_\perp)]^2[G^2(I_\parallel + B_\parallel) + 4(I_\perp + B_\perp)]}{[G(I_\parallel - B_\parallel) + 2(I_\perp - B_\perp)]^4} + \frac{G^2(I_\parallel + B_\parallel) + (I_\perp + B_\perp)}{[G(I_\parallel - B_\parallel) + 2(I_\perp - B_\perp)]^2} \quad (7)$$

In this formulation G, $I_\parallel$, and $I_\perp$ are as above, $B_\parallel$ and $B_\perp$ are the backgrounds for the parallel and perpendicularly emitted light, and C is the background subtracted pre-reaction control total intensity that is used to normalize the data (see Methods). If one collects the total intensity without polarizers, the background subtracted intensity SD, σ_s^2, is simplified to the following:

$$\sigma_i^2 = (I + B)/C^2, \quad (8)$$

where I is the measured intensity (note, if an anisotropy change is occurring simultaneously this is not equivalent to the total intensity, see Appendix), B is the background, and C is the control region measured intensity. In Eq. 7, the error propagation covariance term is not given, yet as pointed out (Wahl 1979), this term is not zero. In this study, the magnitude of the covariance term was examined and found to be insignificant in comparison with the variance terms for stopped- flow anisotropy data.

RESULTS AND DISCUSSION

This section contains examples of the combined analysis applied to stopped-flow kinetic reactions. The purpose of these examples is to demonstrate the methodology and not to prove reaction mechanisms for any of the systems discussed. Although all the cases utilized use simple kinetic schemes, the combined analysis methodology will be equally useful for more complex reactions (i.e., with multiple reversible equilibria or branched reactions).

CASE 1: quantum yield effects on the observed steady-state anisotropy time courses: simulated time courses and experimental examples

The relationship between the total intensity (3) and SSA (4) results in an appreciable difference between total intensity and SSA time courses and reaction rates when there is a significant change in the effective quantum yield (q^{eff}) between reactant and product. As mentioned previously, in these circumstances the SSA time course does not directly represent the change in populations over time. Fig. 1 *A* and *B* illustrate the rate of change of SSA that would be observed for a two-state transition when the q^{eff} of the initial and final states change by: 1.25-, 4-, and 10-fold. One can see that as the difference between q^{eff} values increases, the deviation from single exponential anisotropy (q_2 = 1.0) seen in the absence of an intensity change becomes significant. This deviation from exponentiality also represents a deviation from the true populations of the chemical species. With both increasing and decreasing q^{eff}, the deviation from single exponentiality becomes more extreme. As shown in Fig. 1 *A* in a reaction where the effective quantum yield decreases, the rate of SSA change is slower than the rate of change of the intensity. During reactions where q^{eff} increases (see Fig. 1 *B*), the SSA rate of change is more rapid than the corresponding intensity change.

To quantitate the magnitude of the deviation from exponentiality introduced into SSA data by changes in the q^{eff} of different species, simulated data were generated for reactions with varying q^{eff} values between reactant and product. Data were simulated for a simple two-state reaction in which the intensity is increasing as a single exponential with a rate of 0.05 s^{-1}. Associated with this intensity change is a transition between two states with differing anisotropies (arbitrary

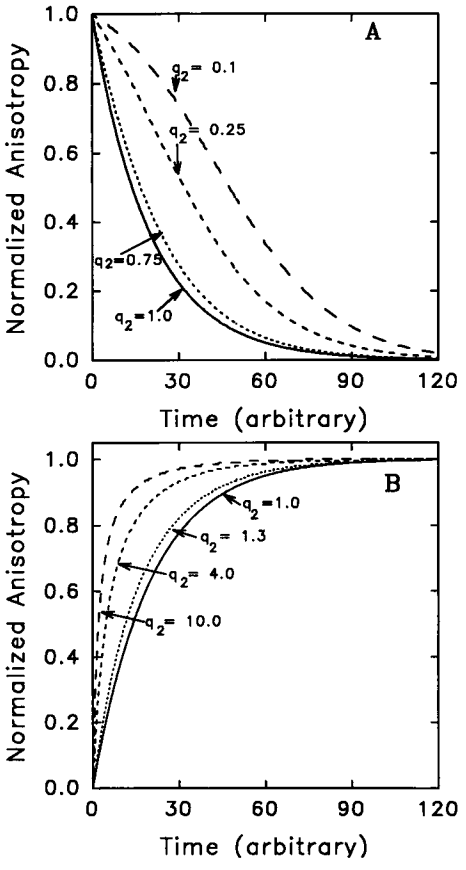

FIGURE 1 Variations in fluorescence anisotropy observable as a function of the effective fluorescence quantum yield. These simulated reaction time courses are for a single transition between two species (Chart I, scheme I) governed by a single exponential change in the intensity observable. For all cases the quantum yield of the reactant (q_1), is 1.0 and the quantum yield of the product (q_2) was varied. Anisotropy is decreasing in *A* and increasing in *B* (units arbitrary). The time courses were generated using Eq. 4 in the text. q_2 equal to 1.0 represents the anisotropy change in the absence of an intensity change. (*A*) Anisotropy observable when fluorescence intensity of the product becomes more quenched: q_2 values are 1.00, 0.75, 0.25, 0.10. (*B*) Anisotropy observable when fluorescence intensity of the product is increasing: q_2 quantum yield values are 1.00, 1.3, 4.0, 10.0.

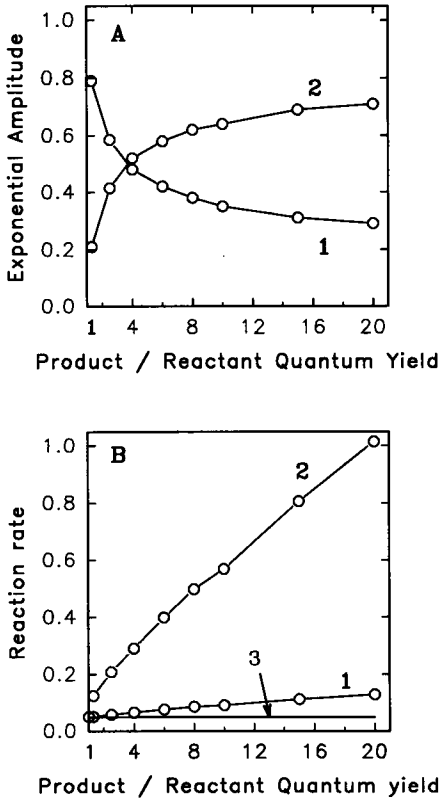

FIGURE 2 Quantitation of the deviations from exponentiality in the steady-state anisotropy observable caused by quantum yield differences between reactant and product. Anisotropy data were simulated using Eq. 4 in text for a two-state reaction (scheme I) involving a single exponential increase in intensity with a rate of 0.05 s^{-1}. Product to reactant effective quantum yield ratios were varied from 1- to 20-fold. These simulated time courses were then analyzed with a sum of two exponentials to obtain amplitudes and rates. (*A*) Amplitudes for the initial (1) and second (2) exponential rate obtained from the anisotropy observable. (*B*) Rates obtained for the initial rate (1) and new exponential rate (2). The intensity reaction rate (0.05 s^{-1}) used to simulate the data is shown (3).

magnitude). The observed anisotropy changes are then analyzed in terms of an empirical sum of two exponentials. From this analysis, *effective* amplitudes and reaction rates were obtained. Fig. 2 *A* shows the rise in amplitude associated with the faster effective rate and a decreased amplitude associated with the initial simulation rate. Even with relatively small changes in the q^{eff} the amplitude of the second exponential is significant. Fig. 2 *B* shows the reaction rates obtained from double exponential analysis of the anisotropy results. The second exponential rate obtained is clearly very dependent on the product/reactant q^{eff}. If the stopped-flow anisotropy data were fit empirically with exponentials, one would conclude that the anisotropy change consisted of two separate phases, instead of a single kinetic phase with the effective quantum yield terms influencing the observable. These data can be very well represented as a sum of two exponentials (with only slight deviations at $q_2 = 20$), even though this is the wrong analytical form for the observable.

Experimentally, the deviation of SSA from the actual populations caused by varying q^{eff} values may alter the ability to observe a reaction or phases in a reaction. For example, if the q^{eff} of the product is much higher than reactant, a very fast reaction might be unobservable, even by rapid stopped flow methods. Alternatively, a reaction involving a substantial decrease in q^{eff} could allow observation of a kinetic process for which the intensity change is too rapid to be followed.

Several experiments were performed with a model protein- folding reaction to demonstrate experimentally the effect of q^{eff} differences on the anisotropy time course and reaction rate. During the unfolding and refolding of a deletion (Δ114–119) mutant of *Staphylococcal* nuclease, the fluorescence of the single tryptophan residue changes ≈2.5-fold. A SSA change of 0.09 anisotropy units accompanies this process. Because easily detectable changes exist for both the total intensity and SSA, this case is an excellent example to evaluate effects of q^{eff} variation upon the SSA reaction rates. The refolding experiment results in an increase in both

fluorescence intensity and SSA and, therefore, the anisotropy time course relative to the intensity time course should be similar to the $q_2 = 4.0$ and $q_2 = 1.0$ time courses in Fig. 1 *B*. Unfolding results in a decrease in both observables and should resemble the $q_2 = 0.25$ and $q_2 = 1.0$ time courses in Fig. 1 *A*. The experimentally measured total-intensity and anisotropy stopped-flow data are shown in Fig. 3.

Empirical exponential analysis of *Staphylococcal* nuclease refolding experiments obtains (Fig. 3 *A*) two exponential reaction rates for both total intensity and SSA. As would be expected from a reaction in which the intensity increases the SSA rates (0.036 and 0.0062 s^{-1}) are faster than those for the total intensity (0.014 and 0.0032 s^{-1}). In the unfolding experiment, a single reaction rate is obtained which, as expected, is slower (0.11 s^{-1}) for the SSA than the corresponding total intensity rate (0.18 s^{-1}). In both cases, the deviations of the SSA time courses and rates from the intensity are significant. It is interesting to note that the unusual deviation from exponentially (i.e., slightly sigmoid shape) predicted by the simulation in Fig. 1 *A* for the anisotropy observable in a case with decreasing intensity is indeed observed in the unfolding experiment.

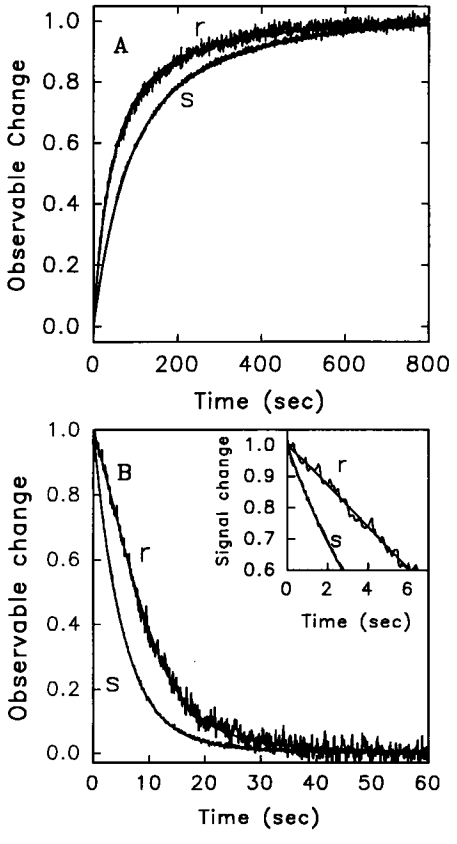

FIGURE 3 Time course of *Staphylococcal* nuclease mutant (Δ114–119) unfolding or refolding as followed by intrinsic tryptophan (W140) fluorescence. Optical detection and reaction conditions are as in Methods. Curves represent the normalized changes in anisotropy and intensity during the course of the reactions. Fits through the data were obtained using scheme II. (*A*) Anisotropy (*r*) and intensity (*s*) time courses refolding. Reactions were initiated by a pH jump from 3.2 to 7.0. (*B*) Anisotropy (*r*) and intensity (*s*) time courses for unfolding. Reactions were initiated by a pH jump from pH 7.0 to 3.6. The inset shows early deviation of anisotropy observable from exponentiality.

From empirical sums-of-exponentials analysis it might be concluded that the total intensity and anisotropy were observing different chemical transitions. For example, it might be postulated that the protein rapidly folds up (as evidenced by the faster SSA change), followed by a slower protein "packing" that doesn't effect the overall SSA, but results in a quantum yield change. For the unfolding case, it could be postulated that the tryptophan environment was disrupted more rapidly than the overall structure and, possibly, that two exponential processes were involved in the unfolding of the overall structure. In both of these cases, the results would be misinterpreted.

Because both total-intensity and anisotropy-refolding experiments required two exponentials, the minimal kinetic model needed for these data would require (at least) three states. Kinetic scheme II (Chart I) was applied to this data. By simple examination of the data, it is very difficult to ascertain whether each phase of the total-intensity change and anisotropy change are correctly "advanced" (or "lagged") in the proper manner. It is also very difficult to determine the internally consistent set of kinetic rate constants that adequately describe both data sets. The combined global analysis of these two data sets allows the recovery of internally consistent rate constants and, equally important, the effective quantum yield (q^{eff}) and steady-state anisotropy associated with the intermediate species.

Simultaneous analysis of the two data types (*solid line* in Fig. 3) reveal that the differences between SSA and intensity rates are "lagged" and "advanced" in exactly the manner predicted by Eqs. 3 and 4 and demonstrated in Fig. 1, *A* and *B*. The recovered parameters for this model are shown in Fig. 4 *A*. It is interesting to note that the analysis reveals the presence of a refolding intermediate that is hyperfluorescent (with respect to the final state) and has a large anisotropy. Neither of these results would be apparent through examination of the data sets in isolation. For instance, because the rate from intermediate to native form is >4× faster than formation of the intermediate, the total-intensity kinetics do not reveal that the final stage of the reaction is associated with a decrease in quantum yield (i.e., the intermediate never represents a large enough population to observe both a rise and fall in the total-intensity). A confidence interval analysis (Beechem, 1992a) was performed to determine the level of certainty in the quantum yield and SSA values obtained for the folding intermediate (Fig. 4 *B* and *C*). From this analysis, it is apparent that a unique value for both the SSA and quantum yield for the intermediate (I) can be obtained, distinct from both the native (N) and unfolded (U) states. It is only through the rigorous combination of constraints in the relationships between anisotropy and total-intensity that this additional information can be obtained.

CASE 2: quantum yield increasing with nearly equal reaction rates

In a two-state reaction (scheme I, Chart I) that involves a change in the SSA and intensity observable, an identical reaction profile for both the intensity and anisotropy is not

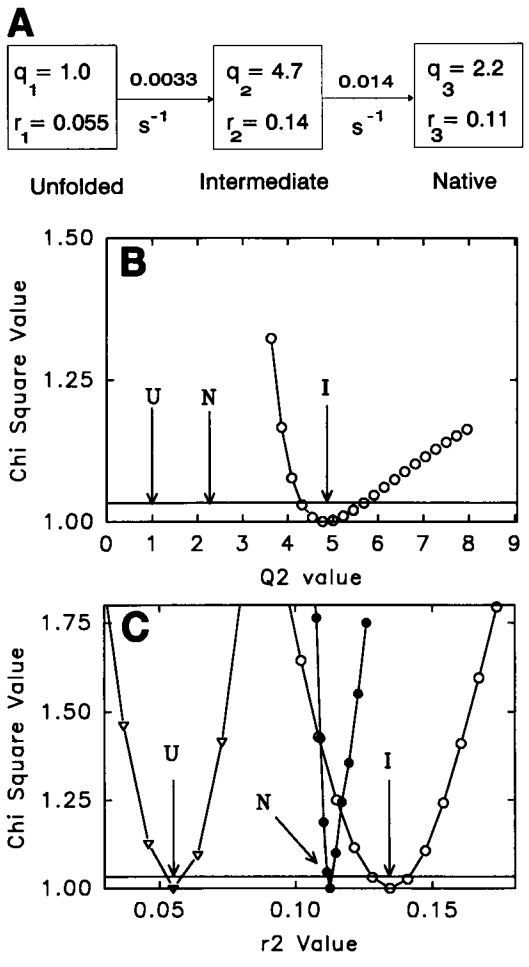

FIGURE 4 Analysis results from refolding experiments with *S.* nuclease using scheme II. (*A*) Rate constants, quantum yield, and steady-state anisotropy results obtained. *B* and *C* represent the confidence intervals associated with the recovered parameters. The horizontal lines represent the approximate 99% confidence level. Values for unfolded (U), native (N), and folding intermediate (I) nuclease are shown. (*B*) Confidence interval result for the quantum yield (q_2) of the intermediate state (confidence levels for the U and N states are within the width of the graphics line). The 99% confidence limit for q_2 is $4.32 < 4.70 < 5.68$. (*C*) Confidence intervals on the recovered anisotropy parameters. Note how the anisotropy for the intermediate state is larger than for the final native state.

possible. If identical kinetics (in terms of effective exponential rates) are observed using both methodologies, then an intermediate (at least a 3-state system) is absolutely required. This is true because of the way in which the magnitude of the change in total intensity influences the anisotropy. Note that this is contrary to expectation, in that identical effective rates observed using two different approaches are often used as evidence to confirm a two- state process. This conclusion, made without understanding the nature of the fluorescence observables, would be exactly wrong.

During the unfolding of yeast phosphoglycerate kinase (PGK) in guanidine hydrochloride (GuHCl), the fluorescence caused by the two tryptophan residues increases threefold. In unfolding experiments with rapid jumps from 0 to 1.4 M GuHCl, the data obtained adequately fit to a single exponential. The observed change in anisotropy and total-intensity when superimposed are virtually identical (Fig.5 *A*). The recovered effective rates are 0.15 ± 0.005 s^{-1} and 0.18 ± 0.001 s^{-1} for the anisotropy and total intensity respectively. Because this experimental case has similar kinetic rates for the SSA and total intensity, one might incorrectly conclude that the unfolding of PGK can be approximated as a two- state reaction. If only total-intensity or anisotropy stopped- flow had been performed, then only two-state behavior would be resolved. Subsequent global analysis of these data sets clearly reveals that two-state behavior does not describe this transition. Examination of the ratio of chisquares for the two- state versus the three-state fit revealed that the three-state fit was superior at greater than 99% confidence level using a nested F-statistic test (Landaw and DiStefano; 1984). Examination of the residual patterns for the analysis of the data for each case yields a very similar conclusion. The insets into the two reaction traces (Fig. 5, *B* and *C*) compare the residuals for analysis using a three-state and two-state (Chart I) scheme. The distorted residual patterns become significantly more random when

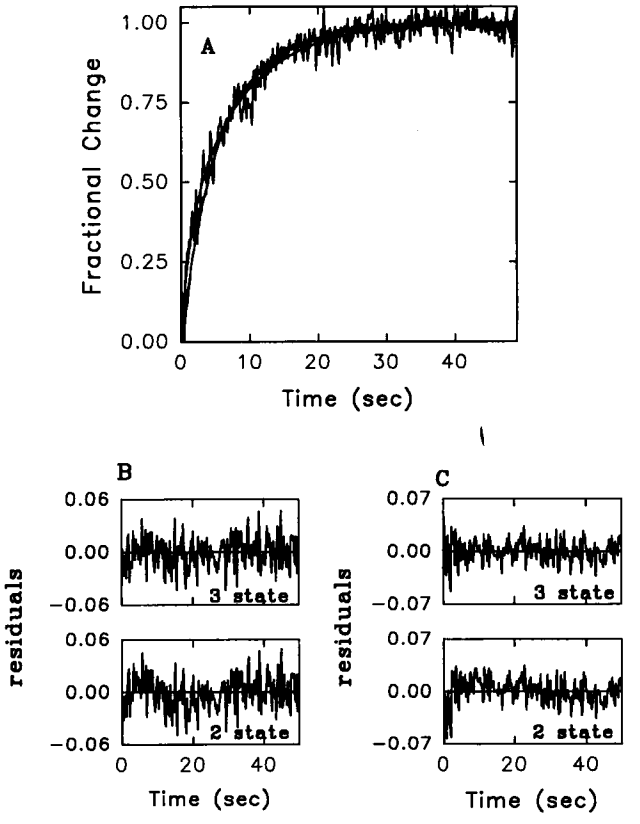

FIGURE 5 Time course of anisotropy and intensity changes during the course of wt phosphoglycerate kinase unfolding. The fluorescence signal monitored is from the two tryptophan residues at positions 308 and 333 and experimental conditions are as described in Methods. Unfolding reactions were initiated by addition of denaturant (GuHCl) to a final concentration of 1.4 M GuHCl and 0.062 mg/ml PGK. (*A*) Overlapping intensity and anisotropy time courses and fits using scheme II. (*B*) Residuals for the intensity analysis using a three-state scheme and a two-state scheme. (*C*) Residuals for the anisotropy analysis using the three-state scheme and two-state scheme.

a three-state model is utilized, predicting an intermediate state associated with the unfolding reaction. Parameters recovered from the three-state analysis predict a very specific reaction in which a hyperfluorescent (relative to the final state) intermediate is formed more slowly ($k_1 \approx 0.11$ s^{-1}) than the exponential rate obtained from empirical exponential analysis. This hyperfluorescent state is then rapidly (≈ 0.25 s^{-1}) converted to a less fluorescent final product. In this particular experiment, the two distinct intensity reaction rates are offset in the anisotropy data by q^{eff} values of the three states such that the time course and rate for the SSA reaction become very similar to those observed for the total intensity. These very specific conditions are necessary to create a case where a three-state transition appears to be a "simple two-state" transition, identical when viewed by either total-intensity or anisotropy. However, neither data set is *internally consistent* with the other. When the data analysis constrains the two measurements to be internally consistent, the "hidden" extra state can be resolved.

CASE 3: uncoupled total-intensity and anisotropy transitions

Examination of the equilibrium unfolding transition in a single tryptophan mutant of PGK (W48) revealed a biphasic total- intensity change with midpoints of approximately 0.4 and 0.9 M GuHCl (Beechem et al., 1994). Performing both total-intensity and anisotropy unfolding experiments using a concentration jump from 0 to 0.5 M GuHCl produced the very striking result shown in Fig. 6, *A* and *B*. One can see that there is a very large bi-phasic total-intensity change (Fig. 6 *B*), however, these transitions have absolutely no effect on the observed anisotropy (Fig. 6 A). In this case, it becomes immediately apparent that the 0.4 M GuHCl transition observed under equilibrium conditions is associated with a "localized" tryptophan photophysical effect, and is not associated with complete (or even partial) unfolding of the protein. This type of uncoupled transition will not present a problem for the described simultaneous data analysis algorithm. A simultaneous fit of these data using scheme II (Chart I; *solid lines* in Fig. 6) revealed a biphasic change in the total-intensity (0.61 and 0.0097 s^{-1}) with equal steady-state anisotropies associated with each of the three states (r_1 = 0.093, r_2 = 0.098, r_3 = 0.103, respectively). In this case, simple collection of both data types was sufficient to resolve the complex equilibrium unfolding profile into two distinct phases: localized "melting" versus global loss of tertiary structure. A complete examination of this mutant and a variety of other single tryptophan mutants of PGK can be found in Beechem et al. (1994)

CASE 4: identification of a unique polymerase-DNA complex

Combined total-intensity and anisotropy analysis is especially useful for cases where the observed total-intensity

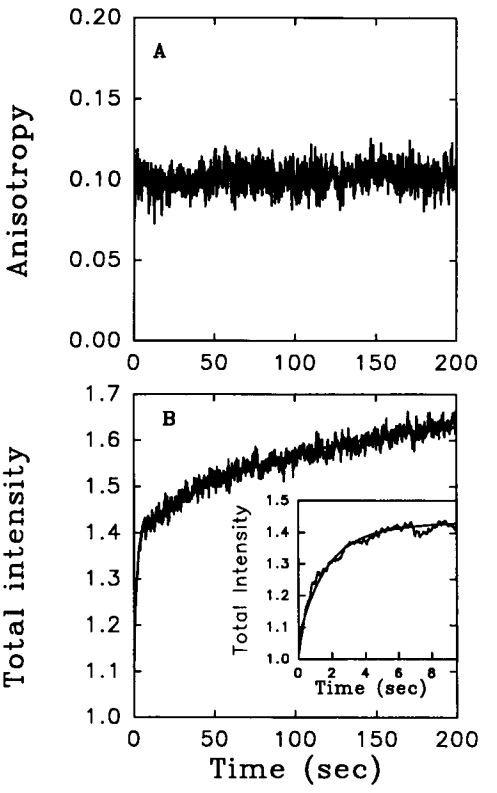

FIGURE 6 Time course of pre-unfolding transition in W48 phosphoglycerate kinase mutant. The fluorescence signal being monitored is from the single tryptophan at position 48. Experimental conditions are as described in Methods. The reaction was initiated by addition of denaturant (GuHCl) to a concentration of 0.5 M GuHCl and 0.1 mg/ml W48 mutant. Analysis of this data was performed using scheme II in Chart I. (*A*) Anisotropy time course and fit. (*B*) Total Intensity time course and fit. The inset shows the initial 10 s of the intensity time course and the fit of this region.

changes are highly complex (e.g., where both transient increasing and decreasing phases are observed). The real-time excision of the fluorescent nucleotide 2-aminopurine (2AP) from primer/template (P/T) DNA by T4 DNA polymerase is a good example of such a reaction. 2AP is highly fluorescent and very sensitive to its environment. When incorporated into double-stranded (ds) P/T DNA, the quantum yield decreases 25- to 125-fold (Bloom et al., 1993; Ward et al., 1969), but when on the 3′ end of the same P/T and bound to T4 DNA polymerase, the 2AP exhibits a fluorescence similar ($\approx$70%) to that of free 2-aminopurine monophosphate (dAPMP). Using this extreme environmental sensitivity, one can follow the kinetics of dAPMP excision from DNA. Examination of the total-intensity stopped- flow time course upon nucleotide excision from the T4 DNA polymerase : ds DNA (T4 DNA) complex reveals that a very rapid fluorescence decrease occurs before a final intensity increase is observed (Fig. 7A). In the absence of additional data, it would be impossible to determine what type of transition is associated with this initial decrease in the fluorescence intensity. Interpretation of the total- intensity data was consistent with a fast transition to a less fluorescent T4-DNA state. If this type of transition was occurring, one would expect that the observed anisotropy associated with this phase

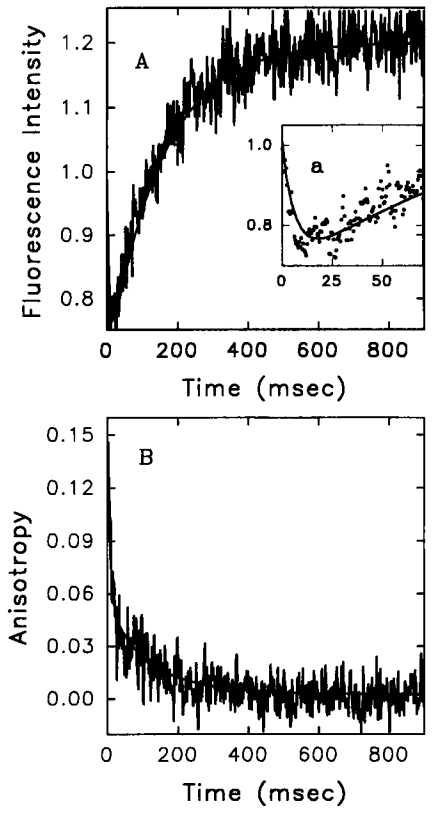

FIGURE 7 Time course of excision of dAPMP from the primer end of primer/template DNA by Bacteriophage T4 DNA polymerase. The fluorescence signal being monitored is from the 2AP fluorescent base at the 3′ end of a P/T within the T4-DNA complex. Experimental conditions are as described in Methods. The excision of dAPMP from pAP/tTT was initiated by addition of $MgCl_2$ to the preincubated T4-DNA complex. Each reaction contained 680 nM T4 Pol, 200 nM DNA, and 8 mM $MgCl_2$. The fit is the best fit using scheme V (chart I). (*A*) Total-intensity time course. Inset *a* shows data and fit for the rapid decrease in fluorescence intensity during the first 75 ms of the reaction. (*B*) Steady-state anisotropy time course and fit.

would either be constant, or increasing. Alternatively, because excised 2AP will have a very low anisotropy value (i.e., freely rotating), rapidly cleaved 2AP would reveal a sharp drop in the observed anisotropy function associated with this rapid phase.

The experimentally observed anisotropy time course (Fig. 7 *B*) shows that ≈75% of the anisotropy decrease occurs during this early phase of the reaction where the total intensity is decreasing. Upon performing a combined analysis of this data using scheme V, a very simple solution to this apparently contradictory data was obtained. Results from these analyses suggest that the decrease in fluorescence intensity results from cleavage of 2AP from a T4-DNA state that is hyperfluorescent relative to excised dAPMP alone. This predicted hyperfluorescent state has since been found experimentally (see Fig. 1 a of Bloom et al., 1994). Results from these analyses suggest at the beginning of the reaction this hyperfluorescent state (species A; scheme V, Chart I) is in equilibrium with a second weakly fluorescent state (B). Rapid formation of the dAPMP product from the hyperfluorescent state results in the decrease in fluorescence intensity and anisotropy. The slow increase in intensity results from rate limiting conversion of the weakly fluorescent T4-DNA complex B to the hyperfluorescent complex A with rapid conversion to dAPMP from this state. This particular model is consistent with that currently proposed in the literature (Capson et al., 1992, Bloom et al., 1994).

CONCLUSIONS

Although stopped-flow SSA and total-intensity studies have been performed for many years, no studies rigorously combining both data types have been described. The prevailing sentiment among kineticists has been to utilize total-intensity measurements whenever possible because the signal magnitude is always larger without polarizers. However, in this work a variety of case studies have been described that reveal the advantages of collecting and analyzing both data types within a single kinetic framework. It has been shown that:

a) Nonexponential steady-state anisotropy kinetics must exist when there is a change in intensity during a reaction. The change in anisotropy will either lag behind or precede the intensity depending upon the nature of the intensity change.

b) Combined analysis can quantitate the relative quantum yields and steady-state anisotropies of intermediate states. The physical properties of the intermediate states are very useful in unravelling the mechanisms involved in biomolecular reactions.

c) This laboratory has been involved in many projects that have resulted in new types of combined global analysis (e.g., Beechem et al., 1991; Beechem, 1992a; Hustedt et al., 1993). What one generally finds is that certain types of combined data sets result in a substantial increase in parameter and model-testing resolution, whereas others result in only a minimal increase in resolution. The combination of total-intensity and anisotropy stopped-flow data sets significantly enhances model testing (e.g., Fig. 5) and parameter resolution (e.g., Fig. 4). Information flow between data sets is very high.

d) Performing kinetic experiments in this manner can provide considerably more insight into the reaction mechanism compared to simple multiexponential analyses of only the total-intensity changes. This additional insight results from information regarding the physical properties of the individual states (i.e., relative quantum yields and steady-state anisotropy values). For instance, the uncoupling of the anisotropy and total-intensity function (Fig. 6) clearly reveals that the initial PGK transition does not involve global unfolding.

It should be mentioned that changes in the observed steady- state anisotropy can be caused by two different effects: the change in rotational motion of the particular species and/or change in the fluorescence lifetime of the species. Because of this, before it can be stated unambiguously that the molecular motion, and therefore size, of an entity is changing, one needs to rule out effects caused by the fluorescence lifetime. Stopped- flow experiments whereby both

total-intensity and anisotropy time-resolved measurements are made on the millisecond time scale are now appearing in the literature that allow for direct testing of the various models (Walbridge et al., 1987; Han et al., 1987; Beechem et al., 1990, 1992b; Jones et al., 1994).

The analysis presented in this paper does not apply any implicit constraints on the steady-state anisotropies associated with any of the intermediate states. One could, in principle, utilize additional relationships in Eq. 4 associated with totally "dynamic" changes in quantum yield (i.e., all changes in intensity are associated with changes in fluorescence lifetime) or totally static changes in quantum yield (i.e., no lifetime effects associated with the quantum yield change). However, in many biological systems, very complex and mixed (both static and dynamic) changes in quantum yield are likely to be observed. Therefore, this program has been developed with no implicit photophysical constraints between quantum yield and steady-state anisotropy. It should be emphasized that the quantum yields obtained from this analysis are all referenced to the quantum yield of the initial (pre-reaction) state. Absolute quantum yields can be obtained by multiplication of the recovered effective quantum yield with the absolute quantum yield of the initial state. Of course, determination of associated emission spectral shifts and extinction coefficient changes for the intermediate state(s) would be required.

e) Subtle polarization bias effects can affect the observed intensity in reactions where a change in anisotropy accompanies the intensity change. Non-zero values of the steady-state anisotropy can affect the observed emission intensity. In reactions where a large change in SSA occurs rapidly, this polarization bias would manifest itself as an additional phase in the total-intensity reaction. The majority of commercial stopped- flows do not take into account this polarization bias term. For those researchers collecting stopped-flow total-intensity data with commercial instrumentation, an Appendix is provided that describes how to evaluate (and correct) the polarization bias of detection. Collecting magic angle-emitted intensity or measurement of the stopped-flow anisotropy allows one to correct polarization bias artifacts (see Appendix).

APPENDIX

In stopped-flow experiments that are performed without polarizers, a non-zero value of the anisotropy function can effect the observed total intensity changes that are observed. During a reaction in which there is a large change in intensity and a corresponding large change in anisotropy, one can observe effects on the observed emitted intensity that originate from changes in the polarized intensity (Weber and Teale, 1957). These effects can appear as an additional small amplitude kinetic phase in the observed total intensity and can be eliminated by collecting data using polarizers under various conditions. One can collect intensity data by exciting with vertically polarized light and collecting the vertical and horizontal emission and calculating the actual total intensity (Eq. 2). However, if an excitation polarizer is lacking, several other alternatives exist. Exciting with natural light and collecting emission with polarizers under "magic angle conditions" or with a polarization scrambling device in the emission channel gives the correct unbiased total intensity (see Badea and Brand (1979) for various cases). When natural (unpolarized) light is used for excitation, the total intensity and anisotropy functions change to (Wahl, 1975):

$$S = 2GI_{\parallel} + I_{\perp} \tag{9}$$

$$r = (GI_{\parallel} - I_{\perp}) / 0.5(2GI_{\parallel} + I_{\perp}) \tag{10}$$

These terms are exactly the same as those in Eq. 2. The 0.5 multiplier term takes into account the differences between the vertical and natural light excited total intensities. As a final alternative, the quantitative effects of this non-zero steady- state anisotropy on the observed emitted intensity can be corrected using the method of Cehelnik et al. (1975). In this case, one must measure the stopped-flow anisotropy change. The measured anisotropy change can then be directly utilized to correct the polarization bias term associated with a total- intensity experiment performed without polarizers.

For example, the observed total intensity when using completely unpolarized excitation is

$$I_o(t) = I^u_o(t)/(1 - r(t)/4), \tag{11}$$

where I^u_o is the uncorrected observed intensity, I_o is the intensity corrected for polarization effects, $r(t)$ is the measured stopped- flow anisotropy of the reaction. The majority of stopped-flow fluorescence intensity studies do not mention whether they have evaluated the effects of anisotropy changes. Some may incorrectly conclude that a particular reaction phase exists, when indeed the phase may be caused solely by the effect of a large anisotropy change. Although in many cases the effects seen are small, the anisotropy changes must be investigated for this to be known.

This work was supported by grants from National Institutes of Health (GM45590) and the Lucille P. Markey Charitable trust, and by a National Institutes of Health training grant. T 32GM08320 (M. R. Otto). J. M. Beechem is a Lucille Markey Scholar in Biomedical Sciences. M. P. Lillo acknowledges the support of C.S.I.C. and a fellowship from M.E.C. (Spain).

REFERENCES

Badea, G., and L. Brand. 1979. Time-resolved fluorescence decay measurements. *Methods Enzymol.* 61:378–425.

Beechem, J. M., L. James, and L. Brand. 1990. Time-resolved fluorescence studies of the protein folding process: new instrumentation, analysis, and experimental approaches. *In* Time-Resolved Laser Spectroscopy in Biochemistry II. J. R. Lakowicz, editor. SPIE proceedings 1204:686–698.

Beechem, J. M., E. Gratton, M. Ameloot, J. R. Knutson, and L. Brand. 1991. The global analysis of fluorescence intensity and anisotropy decay data: second-generation theory and programs. *In* Topics in Fluorescence Spectroscopy, Vol. 2. J. R. Lakowicz, editor. Plenum Press, New York.

Beechem, J. M. 1992a. Global analysis of biochemical and biophysical data. *Methods Enzymol.* 210:37–53.

Beechem, J. M. 1992b. Multi-emission wavelength picosecond time-resolved fluorescence decay data obtained on the millisecond time scale: application to protein: DNA interactions and protein folding reactions. *In* Time-Resolved Laser Spectroscopy in Biochemistry III. Joseph R. Lakowicz, editor. SPIE proceedings 1640:676–681.

Beechem, J. M., M. A. Sherman, and M. T. Mas. 1995. Time- resolved and stopped-flow kinetic measurements of fluorescence intensity and anisotropy changes during unfolding of several single tryptophan mutants of phosphoglycerate kinase. Biochemistry. In press.

Bevington, P. R., and D. K. Robinson. 1992. Data Reduction and Error Analysis for the Physical Sciences. McGraw-Hill, Inc., New York.

Bloom, L. B., M. R. Otto, J. M. Beechem, and M. F. Goodman. 1993. Influence of 5′-Nearest neighbors on the insertion kinetics of the fluorescent nucleotide analog 2-aminopurine by Klenow fragment. *Biochemistry.* 32:11247–11258.

Bloom, L. B., M. R. Otto, R. Eritja, L. J. Reha-Krantz, M. F. Goodman, and J. M. Beechem. 1994. Pre-steady state kinetic analysis of sequence dependent nucleotide excision by the 3′-exonuclease activity of bacteriophage T4 DNA polymerase. *Biochemistry.* 33:7576–7586.

Brand, L., J. R. Knutson, L. Davenport, J. M. Beechem, R. E. Dale, D. W. Walbridge, and A. A. Kowalcyzk. 1985. Spectroscopy and the Dynamics of Molecular Biological Systems. P. M. Bayley and R. E. Dale, editors. Academic Press, New York.

Capson, T. L., J. A. Peliska, B. F. Kaboord, M. W. Frey, C. Lively, M. Dahlberg, & S. J. Benkovic. 1992. Kinetic characterization of the polymerase and exonuclease activities of the gene 43 protein of bacteriophage T4. *Biochemistry.* 31:10984–10994.

Cehelnik, E. D., K. D. Mielenz, and R. A. Velapoldi. 1975. Polarization effects on fluorescence measurements. *J. Res. Natl. Bur. Stand.* 79A:1–15.

Dandliker, W. B., J. Dandliker, S. A. Levison, R. J. Kelly, A. N. Hicks, & J. U. White. 1978. Fluorescence methods for measuring reaction equilibria and kinetics. *Methods Enzymol.* 48:380–415.

Dandliker, W. B., M. Hsu, J. Levin, and B. R. Rao. 1981. Equilibrium and Kinetic Inhibition Assays Based upon Fluorescence Polarization. *Methods Enzymol.* 74:3–28.

Eftink, M. R. 1994. The use of fluorescence methods to monitor unfolding transitions in proteins. *Biophys. J.* 66:482–501.

Han, M. K., D. G. Walbridge, J. R. Knutson, L. Brand, and S. Roseman. 1987. Nanosecond time-resolved fluorescence kinetic studies of the 5,5′-Dithiobis-(2-nitrobenzoic acid) reaction with Enzyme I of the phosphoenolpyruvate: glycose phosphotransferase system. *Anal. Biochem.* 161:479–486.

Hustedt., E. J., C. E. Cobb, A. H. Beth, and J. M. Beechem. 1993. Measurement of rotational dynamics by the simultaneous nonlinear analysis of optical and EPR data. *Biophys. J.* 64:614–621.

Jones, B. E., J. M. Beechem, and C. R. Matthews. 1995. Local and global dynamics during the folding of *E. coli* dihydrofolate reductase by time-resolved fluorescence spectroscopy. *Biochemistry.* In press.

Landaw, E. M., and J. J. DiStefano III. 1984. Multiexponential, multicompartmental, and noncompartmental modeling. II. Data analysis and statistical considerations. *Am. J. Physiol.* 246(Regulatory Integrative Comp. Physiol. 15):R665-R677.

Levison, S. A. 1975. Fluorescence polarization kinetic studies of macromolecular reactions. *In* Biochemical Fluorescence: Concepts, Vol. 1. R. F. Chen and H. Edelhoch, editors. Marcel Dekker, New York.

Ludescher, R. D., L. Peting, S. Hudson, and B. Hudson. 1987. Time-resolved fluorescence anisotropy for systems with lifetime and dynamic heterogeneity. *Biophys. Chem.* 28:59–75.

Walbridge, D. G., J. R. Knutson, and L. Brand. 1987. Nanosecond time-resolved fluorescence measurements during protein denaturation. *Anal. Biochem.* 161:467–478.

Wahl, P. 1975. Decay of fluorescence anisotropy. *In* Biochemical Fluorescence: Concepts, Vol. 1. R. F. Chen and H. Edelhoch, editors. Marcel Dekker, New York

Wahl, P. 1979. Analysis of fluorescence anisotropy decays by a least square method. *Biophys. Chem.* 10:91–104.

Ward, D. C., E. Reich, and L. Stryer. 1969. Fluorescence studies of nucleotides and polynucleotides. I. Formycin, 2- aminopurine riboside, 2,6 diaminopurine riboside, and their derivatives. *J. Biol. Chem.* 244: 1228–1237.

Weber, G., and F. W. J. Teale. 1957. Determination of the absolute quantum yield of fluorescent solutions. *Trans. Faraday Soc.* 53: 646–655.